

Tetrahedral structure of supercooled water at ambient pressure and its influence on dynamic relaxation: Comparative study of water models



Yu-Wei Kuo^a, Ping-Han Tang^{a,1}, Hao Wang^a, Ten-Ming Wu^{a,*}, Shinji Saito^{b,c}

^a Institute of Physics, National Yang Ming Chiao Tung University, Hsinchu 30010, Taiwan

^b Institute for Molecular Science, Myodaiji, Okazaki, Aichi 444-8585, Japan

^c The Graduate University for Advanced Studies, Myodaiji, Okazaki, Aichi 444-8585, Japan

ARTICLE INFO

Article history:

Received 5 April 2021

Revised 29 July 2021

Accepted 10 August 2021

Available online 25 August 2021

Keyword:

Supercooled water

Tetrahedral structure

Relaxation time

Excess entropy

ABSTRACT

In this paper, we investigated the tetrahedral structure of supercooled water at ambient pressure and its influence on dynamic relaxation by comparing simulation results of TIP4P/2005 and SPC/E water models. The globally tetrahedral structure of supercooled water was characterized with the second-peak maximum and a deep first minimum in the radial distribution function $g(r)$ of O-atoms and the reverse order in magnitude between the first two peaks of structure factor. The locally tetrahedral structure was specified by molecules, which and their neighbors up to the second hydration shell all have four H-bond coordinators. These molecules are referred as low-density liquid (LDL) and the others as high-density liquid (HDL). The water dynamics relaxation was studied through the self-intermediate scattering function, the non-Gaussian parameter, and the polarizability anisotropy time correlation function. Indicated by our simulations, the temperature dependence of the stretched exponent describing the α -relaxation displayed a small peak in the supercooled regime above the Widom line (WL), where LDL at the peak temperature was roughly one fourth of the total. The stretched exponent depicting the polarizability anisotropy relaxation was found to be insensitive to temperature, consistent with the experimental results. Above the WL, all relaxation times studied displayed a power-law temperature dependence with a consistent singular temperature for each model. The inverse relaxation times showed exponential functions of two-body excess entropy due to translational motions, where the entropy exhibited a logarithmic temperature behavior with a singular temperature close to that of relaxation time. This result leads to a conclusion that excess entropy is a quantity to describe dynamic relaxation of supercooled water in the thermodynamic region where the mode-coupling theory works. The water structure that causes the two-body excess entropy is illustrated and the contributions of HDL, LDL, and their mixing are also shown, where the mixing contributes significantly as near the WL. Below the WL, the formula based on the two-body excess entropy may no longer be valid.

© 2021 Elsevier B.V. All rights reserved.

1. Introduction

Water is well known for many anomalous behaviors relative to simple liquids, having influences on our daily life and chemical, biological, and geological processes [1]. At ambient pressure (AP), water exhibits a density maximum at 4 °C. Below the melting point, the isothermal compressibility, isobaric heat capacity, and the magnitude of thermal expansion coefficient of supercooled water increase dramatically upon cooling [2,3] and seem to diverge in a power law near 228 K [4]. Though several scenarios have been proposed to explain these anomalies [5–9], the origin to cause

them is still elusive, because of homogeneous nucleation to ice near $T_H \approx 235\text{K}$, hindering our understanding about supercooled water below T_H .

The existence of two distinct local structures in supercooled water was suggested by experiments [10–12] and simulation studies [13–17]. The two forms of local structure are characterized with tetrahedrally ordered H-bonds and strongly distorted H-bonds [3,10]. In the liquid–liquid transition (LLT) scenario [18,19], supercooled water at low pressure can be described as a mixture of the two forms of local structure, which are interconvertible. Upon cooling, the mixture transforms in structure continuously from the strongly-distorted form to the tetrahedrally-ordered one, whereas thermodynamic response functions of the mixture, such as isothermal compressibility and isobaric heat capacity, exhibit maxima as the fractions of the two forms are almost equal

* Corresponding author.

E-mail address: tmw@faculty.nctu.edu.tw (T.-M. Wu).

¹ Present address: Research Center of Applied Science, Academia Sinica

[16,20]. By increasing pressure, the loci of these thermodynamic maxima merge on a single line, referred as the Widom line (WL) [21], in the P - T plane. The WL approaches to a critical point, near which the thermodynamic maxima diverge. Above the critical pressure, the two forms of local structure segregate into two metastable phases separated by a coexistence line [22]. The two phases are referred as low-density liquid (LDL) and high-density liquid (HDL), which correspond to two basins in the free energy surface of metastable water [23]. The coexistence line of the two liquids is an extension of the first-order phase transition between their counterparts, low-density and high-density amorphous ices observed in laboratories [24].

Embedded in deeply supercooled regime, the liquid-liquid critical point (LLCP) of supercooled water is inaccessible experimentally, and its existence is only predicted by simulations for a few models with rigorous analyses for criticality [25,26]. So, the LLCP scenario of supercooled water is still hypothetical [9]. Recently, the water-droplet experiment at AP shows maxima in isothermal compressibility and correlation length of deeply supercooled water at 229 K [27], indicating the existence of the WL. The appearance of these maxima is associated with the fast growing of tetrahedral order in water structure, extending up to the second hydration shell of a molecule [28,29]. Furthermore, the isobaric heat capacity of water droplet also displays a maximum at 228 K [30], and the LLT of supercooled water is illustrated experimentally [31].

On dynamic aspects, the self-diffusion coefficient of supercooled water at AP exhibits a power-law temperature dependence with a singularity near 228 K [2,4], like the observed behaviors of thermodynamic responses. By molecular dynamics (MD) simulations [32–36], the power-law behavior also reflects on relaxation time of translational dynamics in mild supercooled water. In relation to thermodynamics, a semi-empirical scaling relationship between diffusion coefficient and excess entropy has been proposed for many liquid systems [37–42], where excess entropy is related to structural correlation due to molecular interactions. In the last decade, a relationship to excess entropy has been extended to relaxation time of liquid dynamics [43,44]. Recently, the relationship was found to work for translational dynamics in supercooled water above the WL, with the excess entropy replaced by its two-body contribution [45,46].

In this paper, we investigated the tetrahedral structure, up to the second hydration shell, of supercooled water at AP, and its influence on relaxation times of dynamic properties, including translational molecular motions, the non-Gaussian parameter [47], and the polarizability anisotropy dynamics, where the last one can be measured by the time-resolved optical-Kerr-effect spectroscopy [48], which provides an indication for two distinct local structures in supercooled water [12]. All results studied were compared between TIP4P/2005 [49] and SPC/E [50] water models: The former shows stronger tetrahedral order in local structure and possesses a LLCP, which is accessible by simulations recently [26], whereas the latter exhibits weaker tetrahedral order and has no strong evidence for the occurrence of a LLCP [51,52]. To examine the polarizability anisotropy dynamics, we amended the two water models with the same collective polarizability model [53] for assuring that their differences in the related dynamics come from the distinction between their local structures.

All investigated relaxation times of supercooled water above the WL were found to show a power-law temperature dependence and their inverses exhibit exponential functions of the two-body excess entropy of water structure. At room temperatures, the two-body excess entropy is resulted from the excluding effect due to molecular size and the local order of molecules within the first hydration shell. As the tetrahedral order is developed in space at supercooled conditions, extra contributions come from molecular order in the second hydration shell and vacancies around inter-

stitial sites in 3D tetrahedral structure [54]. The paper is organized as follows: Section 2 describes the background of water dynamics and the two-body excess entropy. In Section 3, MD simulations of the two water models are portrayed. The tetrahedrality of water is illustrated for global liquid and for local structure. In Section 4, relaxation times and stretched exponents describing dynamic relaxations are scrutinized. The functions of inverse relaxation times varied with the two-body excess entropy are presented. Conclusions of our studies are given in Section 5.

2. Background of water dynamics

For many years, water dynamics has been a topic of research by experiments and numerical simulations. Above the melting point, the single-molecule translational motion in water, mostly associated with its O-atom, is ballistic initially but then changes to a random behavior through innumerable collisions with other molecules. The random motions cause liquid diffusion and the liquid dynamics entering the diffusive region is referred as the α -relaxation. On cooling into the supercooled regime, a molecule after the ballistic motion is trapped for a period in a transient cage formed by its neighbors and the liquid dynamics within this period is referred as the β -relaxation. The molecular trap is referred as the cage effect, where its influence on ultrafast water dynamics has been studied recently by coherent X-ray scattering [55]. The trapped molecules eventually escape out of their cages through structural relaxation and their motions become diffusive. On the other hand, the polarizability anisotropy dynamics of an asymmetric-molecule liquid is associated with the change in off-diagonal elements of its collective polarizability tensor, caused by reorientations and translations of molecule [48], and the related dynamics provides information on collective orientational dipole relaxation and low-frequency intermolecular vibrations [56–58].

The properties of water dynamics to be studied are described in the following:

A. The self-intermediate scattering function (SISF) [59]

$$F_s(q, t) = \frac{1}{N} \left\langle \sum_{i=1}^N e^{i\vec{q} \cdot \Delta \vec{r}_i(t)} \right\rangle, \quad (1)$$

where $\Delta \vec{r}_i(t) = \vec{r}_i(t) - \vec{r}_i(0)$ is the displacement of O-atom in the i -th molecule at time t and N is the total number of molecule. The brackets in this paper denote an ensemble average at a thermodynamic state. For supercooled water above the WL, the SISF can be depicted by the ideal mode-coupling (MC) theory [60] and is given as

$$f(q, t) = (1 - A_x) \exp \left[-\left(\frac{t}{\tau_G} \right)^2 \right] + A_x \exp \left[-\left(\frac{t}{\tau_\alpha} \right)^{\beta_x} \right], \quad (2)$$

where the first term describes the initial ballistic motions of molecule and the second term portrays the long-time decay of the α -relaxation. A_x is determined by the plateau of the SISF associated with the β -relaxation. For water, the α -relaxation time τ_α is short at room temperatures but extremely long in deeply supercooled regime, overall displaying an inverse-power temperature dependence above the WL.

B. The non-Gaussian parameter (NGP) [47]

$$\alpha_{NG}(t) = \frac{3 \langle |\Delta \vec{r}(t)|^4 \rangle}{5 \langle |\Delta \vec{r}(t)|^2 \rangle^2} - 1, \quad (3)$$

where $\langle |\Delta \vec{r}(t)|^l \rangle$, with $l = 2, 4$, is an average of the O-atom displacement of the l -th power. The NGP is the first correction to the Gaussian approximation of the SISF determined by the mean square displacement $\langle |\Delta \vec{r}(t)|^2 \rangle$, where the Gaussian

approximation works at short times as well as long times. The time profile of $\alpha_{NG}(t)$ exhibits a significant increase during the β -relaxation up to a broad maximum, followed by a relatively slow decay at long time. As approaching to glass transition, the maximum of $\alpha_{NG}(t)$ increases consistently with the growing heterogeneous dynamics, where the time τ_{NG} of the maximum is around the end of the β -relaxation and displays an inverse-power increase on temperature upon cooling [33,61].

C. The polarizability anisotropy time correlation function (PATCF) [56–58]

$$\Psi(t) = \frac{\langle \Pi_{xz}(t)\Pi_{xz}(0) \rangle}{\langle (\Pi_{xz}(0))^2 \rangle}, \quad (4)$$

where Π_{xz} stands for the off-diagonal elements of collective polarizability tensor Π . In this work, Π of water is composed of two parts: the molecular polarizability (MP) and the induced polarizability (IP), where the MP is a sum of the intrinsic polarizabilities of individual molecules and the IP arises from the dipole-induced-dipole interactions between molecules [53,62,63]. For a liquid of rigid molecules, the MP is only related to molecular reorientations, whereas the IP has more relations to translational motions of molecule. For water, $\Psi(t)$ shows a Gaussian decay at short times but then changes to an oscillatory behavior within a time interval depending on liquid temperature, where the oscillations are essentially resulted from intermolecular vibrations [64]. At long times, $\Psi(t)$ decays slowly and can be portrayed by a stretched exponential function given as

$$\Psi(t) \cong A_s \exp \left[- \left(\frac{t}{\tau_s} \right)^{\beta_s} \right], \quad (5)$$

where β_s and τ_s are, respectively, the stretched exponent and relaxation time characterizing the polarizability anisotropy relaxation. A_s is associated with the intermediate-time plateau of $\Psi(t)$ resulted from the cage effect. β_s and τ_s differ in value from β_x and τ_x , respectively, since the PATCF is associated with collective liquid dynamics [65] but the SISF is related to single-molecule dynamics. Measured by the time-resolved OKE experiments [12,66], τ_s of supercooled water shows an inverse-power law on decreasing temperature.

The inverse-power temperature dependences of τ_x , τ_s , and τ_{NG} , with a subscript x as α , s , and NG , respectively, can be commonly described as

$$\tau_x(T) = \tau_{x0} \left(\frac{T}{T_x} - 1 \right)^{-\gamma_x}, \quad (6)$$

where T_x is the singular temperature for the divergence of $\tau_x(T)$ and γ_x is the critical exponent characterizing the divergence. This inverse-power law agrees the prediction of the ideal MC theory for fragile liquids [60].

The similar temperature behaviors of the three relaxation times point to a fundamental origin associated with them. Here, we assume that the inverse relaxation time $\tau_x^{-1}(T)$ has an exponential relation to the two-body excess entropy S_2 per molecule through the equation [45,46]

$$\tau_x^{-1}(T) = B_x e^{C_x S_2 / k_B}, \quad (7)$$

where B_x and C_x are constants depending on a dynamic process and k_B is the Boltzmann constant. S_2 is the two-body term of the multi-particle series expansion of excess entropy $S_{ex} = S - S_{id}$ [67], where S is the liquid entropy and S_{id} is the entropy of a gas of water molecules without interaction at the same temperature. Generally, S_2 is the dominant to S_{ex} , so S_{ex} was simply replaced with

S_2 in many studies [42,44,68]. Thus, Eq. (7) is comparable to an approximation of Rosenfeld relation between diffusion coefficient and excess entropy [37,38].

In relation to water structure, S_2 can be evaluated with the radial distribution function $g(r)$ of O-atom

$$\frac{S_2}{k_B} = -2\pi\rho \int_0^\infty [g(r) \ln g(r) - (g(r) - 1)] r^2 dr, \quad (8)$$

where ρ is liquid density. Based on the assumption on relaxation time, S_2 of supercooled water above the WL can be casted into a logarithmic function of temperature in the formula

$$\frac{S_2}{k_B} = \eta + \zeta \ln \left(\frac{T}{T_0} - 1 \right), \quad (9)$$

with three parameters η , ζ , and T_0 , where T_0 is the lower limit that the formula is applicable. A combination of the inverse-power law in Eq. (6) and the assumption in Eq. (7) gives $\eta = -\ln(\tau_{x0} B_x) / C_x$, $\zeta = \gamma_x / C_x$, and $T_0 = T_x$. But, we consider them as fitting parameters for the temperature behavior of S_2 calculated via Eq. (8).

In the next section, molecules in simulated water were classified into HDL and LDL with molecular fractions f_H and f_L , respectively, where $f_H + f_L = 1$. By considering water as a mixture of the two types of molecule, indexed with H and L , the two-body excess entropy of the mixture can be separated into three terms as

$$S_2 = f_H S_2^{HH} + f_L S_2^{LL} + 2\sqrt{f_H f_L} S_2^{HL}, \quad (10)$$

with the pair entropy per molecule given as

$$\frac{S_2^{ab}}{k_B} = -2\pi\rho \sqrt{f_a f_b} \int_0^\infty [g_{ab}(r) \ln g_{ab}(r) - (g_{ab}(r) - 1)] r^2 dr, \quad (11)$$

where a and b are either H or L , and $g_{ab}(r)$ is the partial radial distribution function of O-atoms belonging to type a and type b molecules. The formalism in Eq. (10) is similar as that for the structure factor of a mixture of HDL and LDL given in Ref. [53], and the three terms in Eq. (10) correspond to the contributions of HDL, LDL, and their mixing to S_2 .

3. MD simulation and tetrahedral structure

3.1. MD simulation

We performed MD simulations separately with TIP4P/2005 and SPC/E force fields by using the package LAMMPS [69]. In simulations of each water model, 864 molecules were confined in a cubic box satisfied with periodic boundary conditions. The time step of simulation was 1.0 fs and the shake algorithm was employed to constrain the geometry of each molecule. The simulation temperature was controlled through the technique of Nose-Hoover thermostat [70,71]. In the two force fields, the Lennard-Jones (LJ) potential between O-atoms was truncated at 9 Å, and the Columbic potentials were handled normally within this cutoff distance, whereas the long-range forces were evaluated by using the particle-particle and particle-mesh method [72] in an accuracy of 10^{-4} . The system energy and pressure were made up with the long-range corrections. Both NPT and the NVT simulations were carried out for each model, where the NPT simulations determined the system density at 1 atm and the NVT simulations generated configurations for further analyses. Simulations with TIP4P/2005 force field were carried out at seven temperatures from 328 to 230 K, whereas simulations with SPC/E force field were performed at these temperatures and one more at 220 K. The simulation times are given

in Ref. [64] for TIP4P/2005 model and in Table S1 for SPC/E model [73].

3.2. Tetrahedral structure of global water

Produced by our NPT simulations, the density-temperature dependences of SPC/E and TIP4P/2005 models at 1 atm are presented in Fig. S1 [73]. Our results are consistent with reported data, where the temperature of maximum density (TMD) of SPC/E model is close to 240 K and the TMD of TIP4P/2005 model is near 278 K [74]. With generated configurations, the structure of SPC/E water at 1 atm was calculated and the results are presented in Fig. 1, including $g(r)$, coordination number $n(r)$, and structure factor $S(q)$, where $S(q)$ was calculated from Fourier transform of $g(r)$ and the coordination number was evaluated with the equation

$$n(r) = 4\pi\rho \int_0^r dx x^2 g(x), \quad (12)$$

The results regarding the structure of TIP4P/2005 model are shown in Ref. [64]. The two water models display a similar behavior in $g(r)$ except for numerical differences. With r_1 and r_2 , the first- and second-peak positions of $g(r)$, respectively, the ratio r_2/r_1 of each model is close to $\sqrt{8/3}$, which is the quotient of the edge length L to the center-to-vertex distance a of a regular tetrahedron.

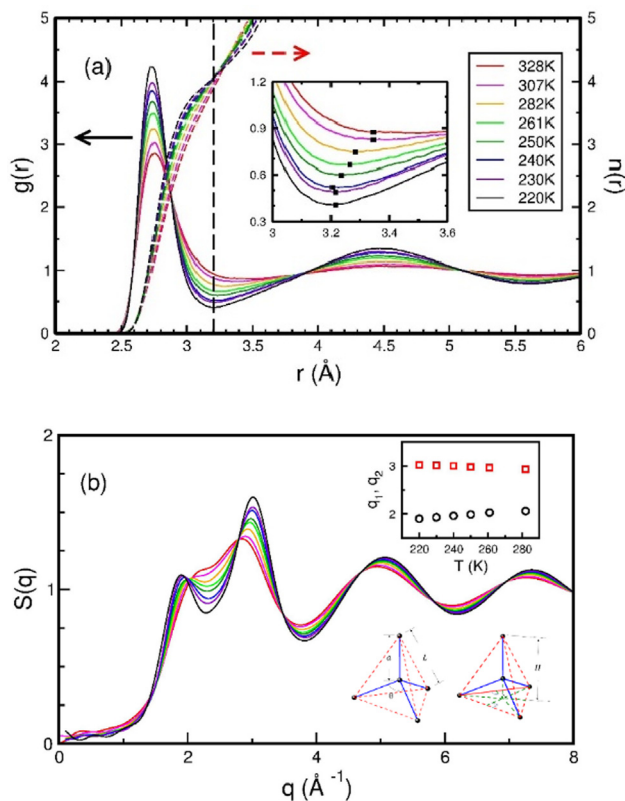


Fig. 1. Structure of SPC/E liquid at 1 atm from 328 to 220 K: (a) radial distribution function $g(r)$ (solid lines) and coordination number $n(r)$ (dash lines), (b) structure factor $S(q)$. All distributions were calculated for O-atoms. In (a), $g(r)$ and $n(r)$ are referred to left and right axes, respectively. The vertical dash line indicates the isobestic point of $n(r)$ at low temperatures. Solid squares in the inset indicate the first minimum in $g(r)$. In (b), the up-right inset presents the temperature dependences of the first-peak position q_1 (circles) and the second-peak position q_2 (squares) of $S(q)$, with q_1 and q_2 in the unit of \AA^{-1} . The lower insets show the structure of a regular tetrahedron, with the center-to-vertex distance a , the edge length $L = \sqrt{8/3}a$, and the tetrahedron height $H = 4a/3$, which is the distance from a vertex to an interstitial site (the crossing of green dash lines). The vertex-center-vertex angle θ is near 109.47° .

Upon cooling, the second peak in $g(r)$ grows, indicating that molecules in water progressively form tetrahedral structure [28,29], whereas the first minimum of $g(r)$ descends and its position moves inwardly as shown in the inset of Fig. 1 (a).

Below the TMD, $n(r)$ shows an isobestic point, indicating the invariance of four coordination numbers within the isobestic-point distance, which is near the first minimum of $g(r)$. The five molecules within the first shell form a tetrahedral structure [75,76] and rearrange their H-bond angles and distances to make the tetrahedral structure more perfect upon cooling, with a consequence of the decrease in water entropy [77]. Above the TMD, the tetrahedral structure is distorted by breaking the connecting H-bonds or the invasion of an interstitial molecule [54].

For SPC/E water at 220 K, the first two peaks of $S(q)$ are located at $q_1 \approx 1.9 \text{ \AA}^{-1}$ and $q_2 \approx 3.02 \text{ \AA}^{-1}$, almost the same positions as TIP4P/2005 model at 230 K [64]. The two peaks become broader as increasing temperature, insomuch that the first peak disappears from $S(q)$ of SPC/E water above 282 K but is still identifiable, though very weak, in $S(q)$ of TIP4P/2005 up to 328 K. Related to structure in real space, the first-peak position is approximately given as $q_1 \approx 3\pi/2r_1$ [78]. By considering that the four nearest neighbors of a molecule form a regular tetrahedron with the center-to-vertex distance a close to r_1 , q_1 can be converted to $2\pi/H$, with $H = 4a/3$ the height of the tetrahedron. Similarly, q_2 is roughly given as $\sqrt{6}\pi/r_1$, which is transformed to $4\pi/L$, with L the edge length of the tetrahedron. Hence, the first and second peaks in $S(q)$ of supercooled water arise, respectively, from density waves in the direction perpendicular to a triangular facet and parallel to an edge of the tetrahedral structure formed by the five molecules within the first shell of $g(r)$.

Both experimental results [75,76] and our model calculations indicate that the second peak in $S(q)$ of supercooled water is higher than the first peak, in a reversed order to the case of simple liquids [59]. As illustrating in Fig. S2 [73], the first peak in $S(q)$ at 220 K is mainly contributed from the second shell of $g(r)$, suggesting that it is important to include the growth of tetrahedral structure (at least) up to the second hydration shell in the definition of LDL of supercooled water. This is consistent with the increase in correlation length further than the first hydration shell by decreasing temperature given in a previous report [79]. However, the second peak in $S(q)$ is resulted from density waves of shell structure in global water so that it has a larger magnitude than the first peak. This anomaly is a common feature of liquids and amorphous materials with tetrahedral structure, like C, Si, Ge, SiO_2 , GeO_2 , etc. [78]. In general, the tetrahedral structure creates vacancies near the interstitial sites, which play a role similar as open local structure for causing the comparable anomaly in structure factors of soft-core liquids without a tetrahedral-like structure [80,81].

3.3. Locally tetrahedral structure

The structures of SPC/E and TIP4P/2005 models are similar in the radial direction as viewing from an O-atom in each liquid, but differ significantly in orientational order in order to elucidate their density differences at supercooled conditions. The orientational order of water structure can be described by the tetrahedral order parameter ξ defined for the arrangement of a molecule and its four nearest neighbors [82]. The difference in orientational order between the two models is illustrated in Fig. 2, where their distributions $P_X(\xi)$ of tetrahedral order parameter are shown at the same temperature and pressure. The comparisons manifest that at any temperature the local structure in TIP4P/2005 liquid has a higher tetrahedral order than that in SPC/E; the $P_X(\xi)$ of SPCE at 240 K still exhibits a small hump at $\xi \approx 0.5$ resulted from strong distortion in local HB network [53]. This explains why the mass

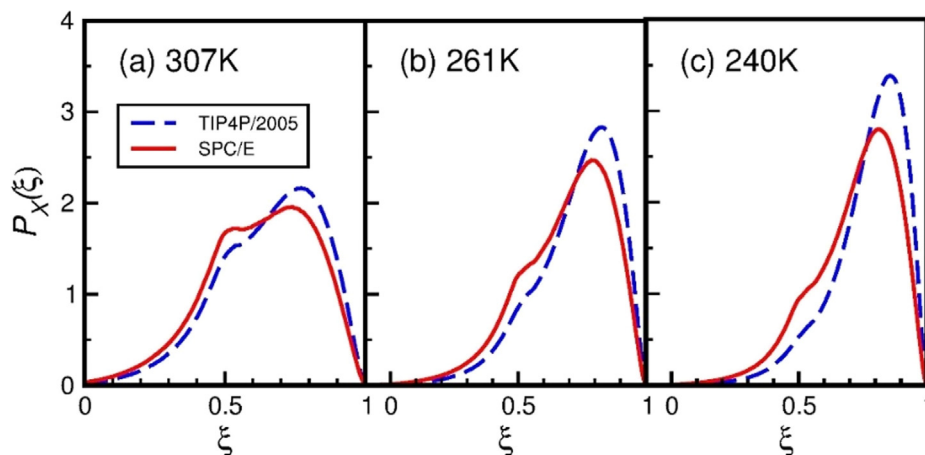


Fig. 2. Comparison of the tetrahedral-order-parameter distribution $P_X(\xi)$ between SPC/E (red solid lines) and TIP4P/2005 (blue dash lines) water at 1 atm: (a) 307 K, (b) 261 K, and (c) 240 K.

density of SPC/E liquid is greater than that of TIP4P/2005 in the supercooled regime.

To examine the tetrahedral order within a space up to the second hydration shell of a molecule, we classified molecules in our simulations into two categories: molecules, which and their neighbors up to the second hydration shell all have four H-bond coordinators, and the others, where a HB is defined by geometric criterions [83]. Classified in this way, the former and latter molecules have lower and higher local densities [17] and, therefore, are referred as LDL and HDL, respectively. According to this classification, molecules of LDL and HDL possess locally tetrahedral structure and locally distorted structure, respectively [17]. By our simulations, the fractions of LDL and HDL in SPC/E and in TIP4P/2005 liquids are shown in Fig. 3, in which the crossover of the two fractions is near 225 K for TIP4P/2005 water, as reported in Ref. [17], but lower than 220 K for SPC/E liquid.

Shown in Fig. 4 are the partial radial distribution functions $g_{HH}(r)$ and $g_{LL}(r)$ of HDL and LDL in SPC/E liquids, respectively, and the pair correlation $g_{HL}(r)$ between the two kinds of molecule, where a small step at the first minimum of a distribution is due to the finite cutoff of a H-bond. The similar distributions of TIP4P/2005 liquid are displayed in Fig. S3 [73]. The sharp first peak in $g_{LL}(r)$ indicates that the four nearest neighbors of a LDL molecule are located in a well-defined distance from the central one, reflecting that the tetrahedral structure of LDL is close to a regular tetrahedron. The shallow first minimum in $g_{HH}(r)$ manifests that HDL includes molecules around the interstitial sites. $g_{HL}(r)$ displays shell structure, but not so sharp as in $g_{LL}(r)$. Similar behaviors in the partial radial distribution functions are shown for HDL and LDL defined in a different method [15].

The local environments of HDL and LDL molecules are further distinguished with order parameters q_3 and \bar{q}_3 defined with the bond orientational order parameter q_{lm} , with $l = 3$ [84], where their definitions are given in Supplementary materials [73]. In terms of q_{3m} defined for a molecule and its first four nearest neighbors, q_3 measures the extent of three-fold orientational symmetry for structural arrangement within the first shell of a molecule. By a similar definition with \bar{q}_{3m} , which is an average of q_{3m} over a molecule and its four nearest neighbors [85], \bar{q}_3 is an average version of q_3 by taking into account the second-shell structure, where \bar{q}_3 is similar as $q_3^{(2)}$ in Ref. [86]. Calculated for perfect tetrahedral structures characterized with full three-fold orientational symmetry, the upper limits of the two parameters are $q_3 = 0.745$ and $\bar{q}_3 = 0.447$.

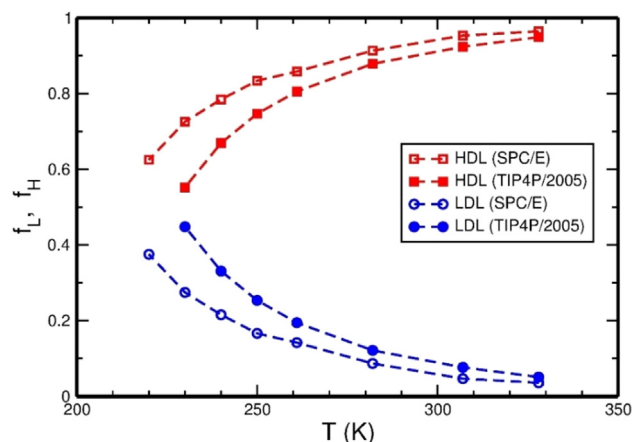


Fig. 3. Fractions of LDL (circles) and HDL (squares) in a water model at 1 atm. The open and filled symbols are for SPC/E and TIP4P/2005 models, respectively, with the dash lines guiding the eye. LDL and HDL molecules, indexed with L and H , have locally tetrahedral and distorted structures, respectively.

Fig. 5 (a) and (b) present, respectively, the distributions of q_3 and \bar{q}_3 calculated for HDL and LDL in TIP4P/2005 liquid. Generally, the q_3 distribution, $P_Q(q_3)$, is similar in behavior as $P_X(\xi)$ [86]: $P_Q(q_3)$ of LDL has a narrow width with a peak close to its upper limit, indicating that the first-shell structure of LDL has a higher three-fold orientational symmetry, whereas the distribution of HDL is more spread and shows a hump near $q_3 \approx 0.4$, revealing a lower three-fold orientational symmetry within the first shell of HDL. The temperature variation of $P_Q(q_3)$ is similar as $P_X(\xi)$ of LDL and HDL classified with another definition [53]. By including the second hydration shell, the behavior of the \bar{q}_3 distribution, $P_Q(\bar{q}_3)$, is different from that of $P_Q(q_3)$, by displaying a more symmetric function about its maximum around $\bar{q}_3 \approx 0.2$. Upon cooling, $P_Q(\bar{q}_3)$ of the global liquid shifts toward its upper limit and becomes somewhat broader due to the developed tetrahedral order in local structure. At each temperature, the $P_Q(\bar{q}_3)$ distributions of LDL and HDL strongly overlap, with the peak of LDL at a slightly higher \bar{q}_3 , and their behaviors are similar as the $q_3^{(2)}$ distributions of ST2 water at temperatures below and above its liquid-liquid transition line [86]. The difference in $P_Q(\bar{q}_3)$ between HDL and LDL reveals that their local structures up to the second

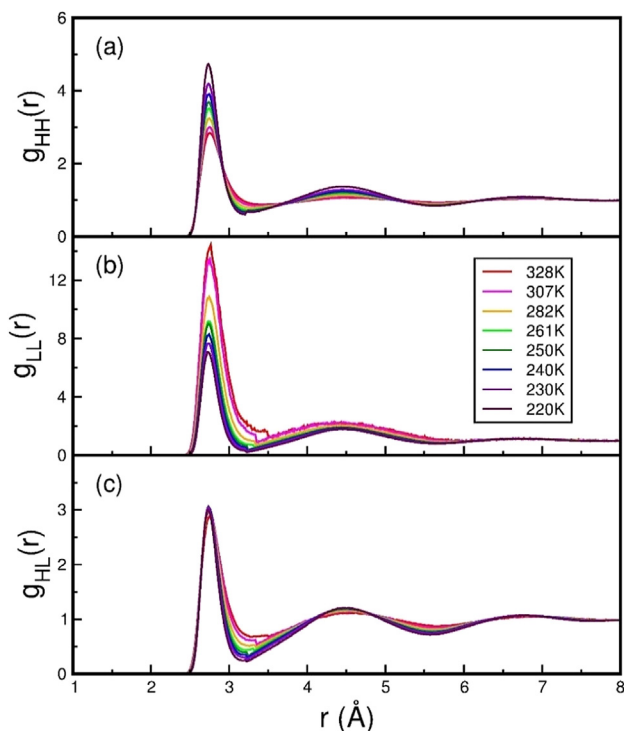


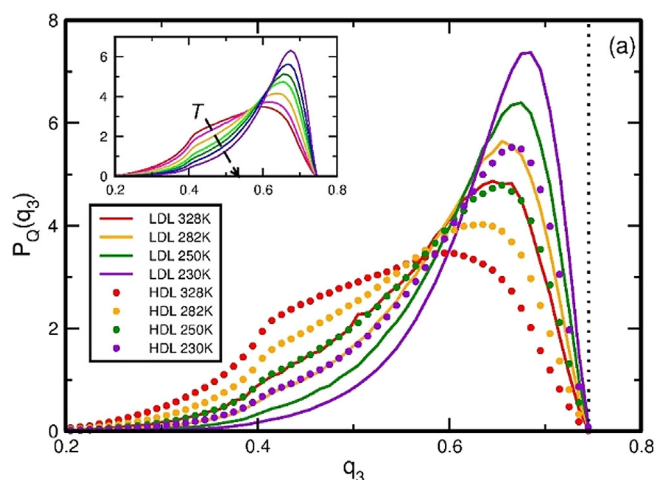
Fig. 4. Partial radial distribution functions $g_{HH}(r)$ and $g_{LL}(r)$ of O-atoms in HDL and LDL, respectively, and the pair correlation function $g_{HL}(r)$ between the two kinds of molecule. The results were calculated for SPC/E liquids at 1 atm.

hydration shell are distinct in the three-fold orientational symmetry, which is a typical feature of a tetrahedron. In a remark, another parameter to distinguish HDL and LDL is related to the torsion via the dihedral angle of two tetrahedral water molecules connected with a H-bond [87], but this approach is beyond the scope of this paper.

4. Relaxation of water dynamics

4.1. Temperature dependence

Displayed in Fig. 6 are dynamic properties of SPC/E water at 1 atm, including the SISFs $F_s(q, t)$ evaluated at q_1 and at q_2 of



$S(q)$, the NGP $\alpha_{NG}(t)$, and the PATCF $\Psi(t)$, where $F_s(q, t)$ at q_1 above 282 K was calculated with q_1 of 282 K due to the first-peak disappearance from $S(q)$. The corresponding dynamic properties of TIP4P/2005 water are presented in Fig. S4 [73]. In Fig. 6 (a), the SISFs at q_1 were fitted by using Eq. (2). For the SISFs at q_2 , the first term in Eq. (2) only gave an approximation at short times [32]; however, the behavior at times over 0.3 ps can be fitted by using the second term, with A_x set at 0.5 ~ 0.6, and the results are shown in Fig. 6 (b). In Fig. 6 (d), the PATCFs at times over 0.2 ps were fitted by using Eq. (5). Through the fitting, the stretched exponents and relaxation times of these dynamic properties were obtained.

The wavevector q that the SISF is calculated selects a length scale $2\pi/q$ to measure local structure of a liquid. Within a domain of this length scale, the random motions of particles at long times result in a single exponential decay of the SISF evaluated for the particles inside. However, different domains of this length scale in a liquid give rise to relaxation times varying with local environments, and the SISF of the liquid is a sum of multiple exponential functions, where the sum yields a stretched exponential function with an exponent β_x characterizing the structural heterogeneity in this length scale. This stretched exponential decay is referred as the spatially heterogeneous dynamics [88]. For water, the length scale determined by the first peak of $S(q)$ is roughly the height H of a tetrahedral unit in the HB network, and the length scale determined by the second peak is nearly a half of the edge length L of the tetrahedral unit, where H is comparable to the distance at the first minimum of $g(r)$ and $L/2$ is slightly shorter than the first-peak distance r_1 .

Fig. 7 shows the temperature dependences of the stretched exponents β_x of the SISF and β_s of the PATCF, in comparisons between SPC/E and TIP4P/2005 models. At any temperature, β_x at q_2 has a smaller value than that at q_1 , because local structure is more heterogeneous as viewed in a shorter length scale. At the same q , β_x of TIP4P/2005 is smaller than that of SPC/E, for the structural heterogeneity of TIP4P/2005 liquid is stronger due to its higher tetrahedral order. At temperatures above 282 K, our results indicate that for both models β_x decreases with temperature, similar as the predictions of previous simulation studies [32–34]. At such high temperatures, the LDL molecules are rare and the number of their clusters is quite low [17] so that their effects on local structure can be negligible and water can be considered as a “one-component” liquid dominated with HDL. The enhancement of structural heterogeneity in this temperature range is due to the reduction in molecular thermal motions.

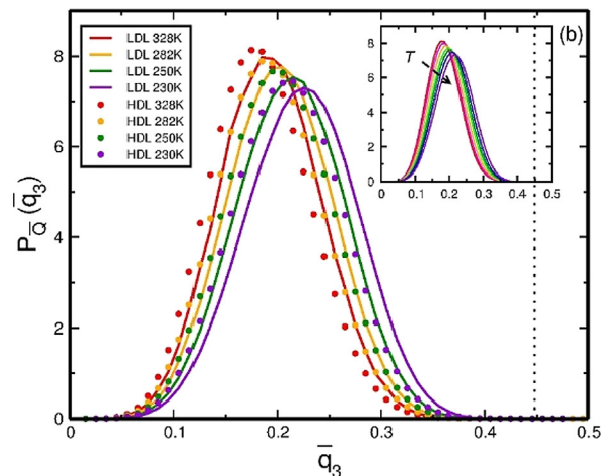


Fig. 5. Distributions of q_3 (a) and \bar{q}_3 (b) calculated for HDL and LDL in TIP4P/2005 water at 1 atm. The dots and solid lines of each color represent the distributions of HDL and LDL at a temperature, respectively, with each distribution normalized to one. In each panel, the inset shows the corresponding distribution of all molecules in the liquid, with the arrow indicating the trend by lowering temperature. The vertical dotted lines in (a) and (b) indicate the upper limit of each order parameter, which is at $q_3 = 0.745$ and $\bar{q}_3 = 0.447$ for perfect tetrahedral structures.

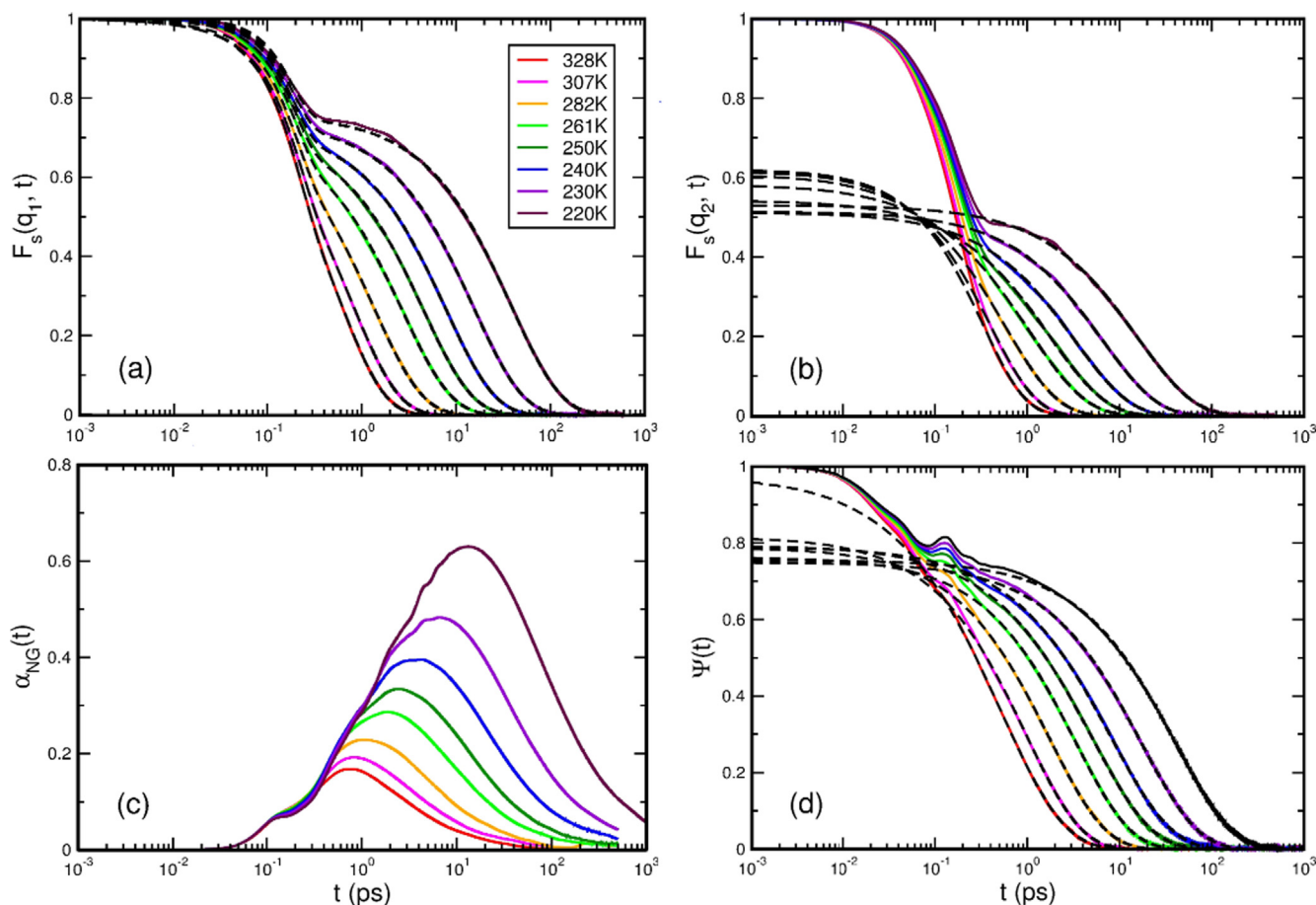


Fig. 6. Dynamic properties of SPC/E liquid at 1 atm with temperature varied from 328 to 220 K: (a) the SISF $F_s(q, t)$ at q_1 , (b) the SISF $F_s(q, t)$ at q_2 , (c) the NGP $\alpha_{NG}(t)$, (d) the PATCF $\Psi(t)$. The solid lines in color are simulation results. The black dash lines are the fitting results by using a function: in (a), Eq. (2) for the full time range; in (b), the second term in Eq. (2) with A_x set at 0.5 ~ 0.6 for times over 0.3 ps; in (d), the stretched exponential function in Eq. (5) for times over 0.2 ps.

Indicated by our results, the variation of β_x below 282 K displays a small peak in each curve of q_1 and q_2 , though very weak in the q_1 curve of SPC/E model, where the peak occurs near 230 ~ 240 K for SPC/E model and near 250 K for TIP4P/2005 model. For both q_1 and q_2 , the peak of TIP4P/2005 liquid is more substantial than that of SPC/E [89]. Near the peak temperature, the LDL molecules in each liquid increase to an amount about one fourth of its total but the number of the LDL clusters decreases so that the structural heterogeneity is somewhat reduced. This partial change from HDL to LDL gives rise to the peak observed in the temperature variation of β_x . Notice that this peak appears at a temperature above the WL and its appearance is distinct from the so-called fragile-to-strong liquid transition [21,90], which occurs near the WL as the fractions of HDL and LDL are almost equal. For SPC/E water above 240 K, its average density still increases with decreasing temperature. This density increase compensates some of the thermal effect so that the structural heterogeneity in the length scale of q_1 is reduced mildly in SPC/E liquid, with a result that only a weak peak is observed in the curve of β_x . At temperatures beyond the peak, the LDL molecules become essential in the HB network and by lowering temperature the thermal effect plays a role again on the increase of structural heterogeneity, which causes β_x to descend.

Shown in Fig. 7 (b), β_s is generally insensitive to temperature for both models, where its average value is near 0.7 for SPC/E model and 0.68 for TIP4P/2005 model, with an error bar of SPC/E somewhat larger than that of TIP4P/2005. The insensitivity of β_s on temperature is consistent with the observation of supercooled water,

where the experimental value of β_s is about 0.6 [12,66]. By comparing β_s and β_x , some remarks can be made. First, in deeply supercooled regime, the average value of β_s is more close to β_x at q_2 , rather than at q_1 . Secondly, owing to a similar behavior of β_s between SPC/E and TIP4P/2005 models, β_s is conjectured to be insensitive to tetrahedral order in water structure but related to the correlation length of the anisotropy collective polarizability, comparable to the length scale of q_2 . The result is consistent with the low collective character of the PATCF [65].

For both water models, the temperature dependence of dynamic relaxation times τ_x can be fitted by using the inverse power law in Eq. (6), with parameters τ_{x0} , T_x , and γ_x given in Table 1, where the data of τ_x at q_1 for TIP4P/2005 liquid are close to the values reported in Ref. [17]. The singular temperatures T_x obtained from each fitting are within a range of 5 K, which is 212 ~ 217 K for TIP4P/2005 liquid and 191 ~ 196 K for SPC/E liquid, except for $T_{NG} \approx 200$ K of SPC/E. For each model, T_x is lower than the WL temperature estimated from the equivalence of the LDL and HDL fractions in Fig. 3. T_x of SPC/E liquid is lower than that of TIP4P/2005; this is consistent with that the melting temperature and TMD of SPC/E are lower than the corresponding values of TIP4P/2005 [74]. Based on the MC theory [60], the singular temperature is due to frozen cage structure.

The validation of the inverse power law for relaxation time is shown in Fig. 8 by the log-log plot of τ_{x0}/τ_x versus $T/T_x - 1$, where the slope of each fitting line gives the critical exponent γ_x . Besides γ_{NG} , γ_x of each model liquid fall in a range, which is 2.6 ~ 3.0 for SPC/E liquid but 2.0 ~ 2.55 for TIP4P/2005 liquid. The different

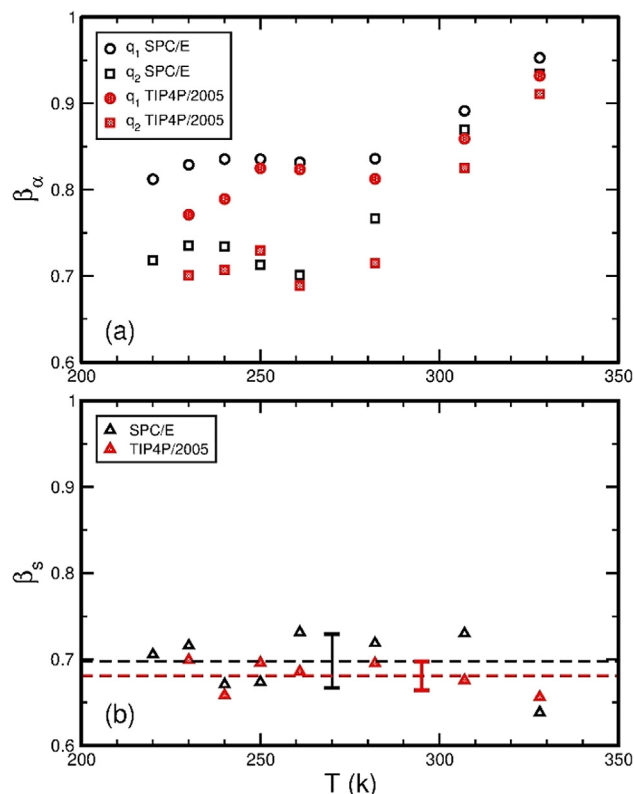


Fig. 7. (a) The stretched exponent β_α of the SISF $F_\alpha(q, t)$ at q_1 (circles) and at q_2 (squares) of $S(q)$, (b) the stretched exponent β_s of the PATCF $\Psi(t)$. The black open and red filled symbols are for SPC/E and TIP4P/2005 models, respectively. In (b), the dash lines indicate the average of β_s with an error bar, which is $\beta_s = 0.70 \pm 0.03$ for SPC/E model and $\beta_s = 0.68 \pm 0.02$ for TIP4P/2005 model.

ranges of the two models indicate that the critical exponent γ_x of water dynamics has some relation to its local structure. γ_α at q_1 is less associated with water structure than γ_α at q_2 , because the length scale of q_1 is longer than that of q_2 . This gives a general trend that the difference in γ_α between SPC/E and TIP4P/2005 models is enlarged, as the measuring length scale is shortened, where the difference of γ_α at q_1 between them is within 0.1 but that of γ_α at q_2 is about 0.5. For the polarizability anisotropy relaxation, the difference in γ_s between the two models is as large as 0.85. In a previous study [53], γ_s is more associated with the induced polarizability of supercooled water, which is resulted from the dipole-induced-dipole mechanism and significantly enhanced by local structure in high tetrahedral order. Thus, γ_s is probably related to the tetrahedral order of water structure. For the maximum of the NGP, γ_{NG} is almost the same for the two models and has a value smaller than other critical exponents studied. Perhaps, the NGP has no specific length scale as for a time correlation function so that γ_{NG} is relatively insensitive to water structure; however, this needs further investigations.

Table 1

Parameters of the inverse power law in Eq. (6) for relaxation times: τ_x of the SISF, τ_s of the PATCF, and τ_{NG} at the maximum of the NGP. All relaxation times were calculated for each model at 1 atm. The SISFs were evaluated at q_1 and q_2 , the first- and second-peak positions of structure factor $S(q)$, respectively. τ_{x0} and T_x are in the unit of ps and Kelvin, respectively.

Model	SISF			PATCF			NGP			
	τ_{x0}	T_x	γ_x	τ_{s0}	T_s	γ_s	τ_{NG0}	T_{NG}	γ_{NG}	
SPC/E	q_1	0.156	196	2.61	0.172	191	2.87	0.246	200	1.72
	q_2	0.055	191	2.98						
TIP4P/2005	q_1	0.104	212	2.53	0.188	217	2.01	0.191	216	1.70
	q_2	0.036	212	2.49						

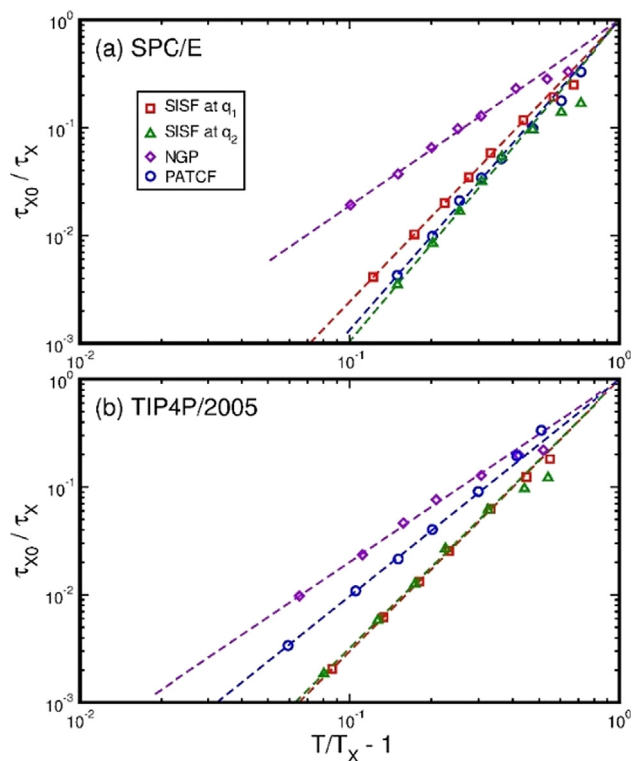


Fig. 8. The rescaling plot of inverse relaxation time versus temperature for SPC/E (a) and TIP4P/2005 (b) models at 1 atm. The time τ_{x0} and temperature T_x for rescaling were obtained from the fitting of τ_x by using Eq. (6). The symbols are simulation data for τ_x of the SISF at q_1 (squares), τ_x of the SISF at q_2 (triangles), τ_{NG} of the NGP maximum (diamonds), and τ_s of the PATCF (circles). The dashed lines are the fitting results.

4.2. Relationship to two-body excess entropy

Presented in Fig. 9 (a) are the two-body entropies S_2 of the two models calculated with $g(r)$ via Eq. (8), where the integration should start from the lower limit at $r = 0$ so that the radial region with $g(r) = 0$ as shown in Fig. S5 [73] yields a nonzero constant to the integration. Physically, this constant to S_2 is due to the excluded volume effect of the LJ repulsive core between O-atoms. In addition to this constant, S_2 at 328 K arises mainly from the local order of molecules within the first shell of $g(r)$. At 220 K, besides the two contributions at high temperatures, extra inputs come from molecular ordering in the second hydration shell and vacancies associated with the first and second minima of $g(r)$, where the vacancies are generally related to the interstitial sites in 3D tetrahedral structure.

At any temperature, the S_2 value of TIP4P/2005 is lower than that of SPC/E. For each model, the temperature variation of S_2 was well fitted by using Eq. (9), with parameters given in Table 2. The singular temperature T_0 , at which S_2 diverges logarithmically,

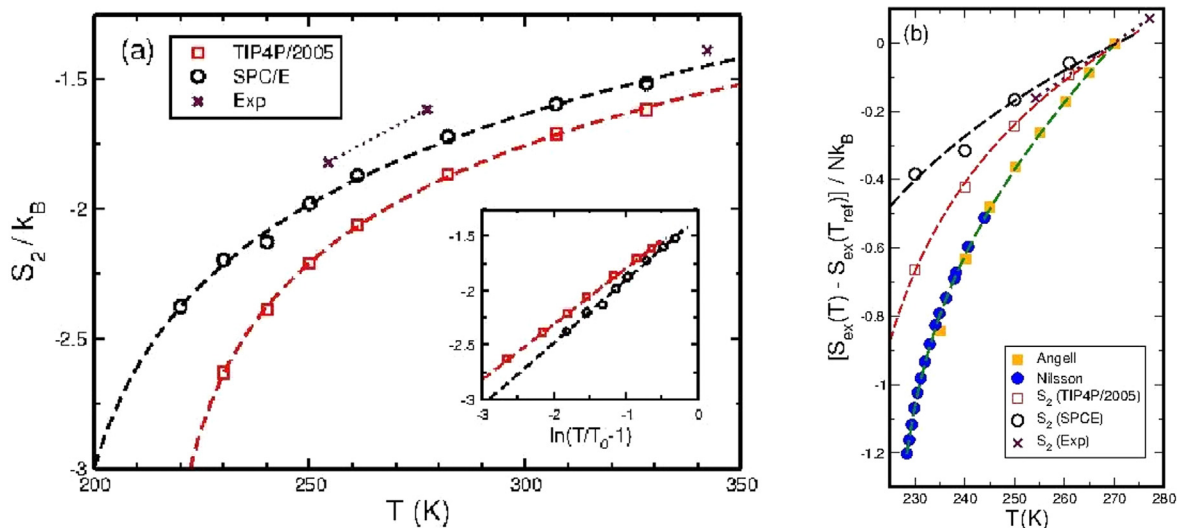


Fig. 9. (a) Two-body excess entropy S_2 as a function of temperature for SPC/E (open black circles) and TIP4P/2005 (open red squares) water systems at 1 atm. (b) Comparison of S_2 with experimental data. The open symbols were S_2 calculated via Eq. (8) for water model systems and the dash lines are the corresponding fitting by using Eq. (9). The maroon crosses were evaluated with experimental densities and the O-O radial distribution functions of real water at 1 bar and $T = 254.2, 277.1$ and 342.7 K [75]. The inset in (a) shows the plot of S_2 as a function of $\ln(T/T_0 - 1)$, with the dashed lines indicating the linear fitting. In (b), the filled symbols are experimental data taken from Ref. [91] for Angell data (orange squares) and from Ref. [30] for Nilsson data (blue circles) measured recently by the ultrafast calorimetry, where the green dash line is the fitting by using a function given in Eq. (S7) [73]. To compare their temperature dependences, all data sets of excess entropy have been shifted by a constant so that their zeros are all located at temperature $T_{ref} = 270$ K.

Table 2

Parameters of two-body excess entropy S_2 in Eq. (9).

Model	η	ζ	T_0 (K)
SPC/E	-1.3184	0.5768	190
TIP4P/2005	-1.2786	0.5114	215

falls into the range of T_x associated with dynamic properties studied, suggesting that T_0 and T_x have the same origin, frozen cage structure. Fig. 9 (b) shows the comparison of S_2 with the excess entropy of supercooled water measured experimentally with respect to its ice crystal [30,91]. The experimental data of excess entropy can be fitted by using a function given in Eq. (S7) [73], similar as Eq. (9) but having an extra linear term of temperature, which might be related to the reference state that the experimental excess entropy is defined with. The experimental excess entropy also shows a logarithmic divergence at T_0 near 225 K, close to the temperature of the maximum isobaric specific heat detected by the ultrafast calorimetry [30]. The experimental T_0 is 10 K above that of TIP4P/2005 water but 35 K above that of SPC/E model, indicating that the former is a more appropriate model to describe supercooled water. The two-body entropies S_2 of real water at three temperatures were evaluated with experimental densities and the O-O radial distribution functions $g(r)$ [75], which are shown in Fig. S7 [73] in comparison with those of the two water models. The experimental S_2 is higher than those of the two water models (but smaller in absolute value), because the experimental $g(r)$ has a lower and broader first peak, increasing the pair entropy due to more disorder in molecular arrangement within the first shell relative to a central one.

In order to compare the temperature dependence of excess entropy, all data set in Fig. 9 (b) have been shifted by a constant so that their zeros are all located at a reference temperature. The two model calculations are deviated from the experimental data, with the calculation of TIP4P/2005 model more close to the data than the SPC/E one. The difference between the experimental data and the model calculation arises from the approximations used in the latter, which involves only the two-body contribution due to

translational motions, whereas beyond this approximation, additional contributions possibly come from orientational motions of molecule [92] and the n -body terms, with $n > 2$, in the multi-particle series expansion of excess entropy [67]. By considering S_2 of real water as a linear function within the range from 254.2 to 277.1 K, the temperature variation of experimental S_2 , after shifting by a constant as shown in Fig. 9 (b), almost agrees with that of TIP4P/2005 water within this temperature range.

In Fig. 10, the inverse relaxation times τ_x^{-1} of dynamic properties are plotted as functions of S_2 for each model, where each τ_x^{-1} was fitted by using Eq. (7) with B_x and C_x given in Table 3. The results of the two models are similar, with the curves of TIP4P/2005 shifting toward lower excess entropy. This reflects that the dynamic relaxation in TIP4P/2005 liquid takes a longer time than that in SPC/E liquid, because the higher tetrahedral order in TIP4P/2005 water makes its local structure more persistent. Based on the results in Fig. 10, the inverse relaxation times associated with the SISF, the PATCF, and the NGP of water dynamics can be portrayed as exponential functions of S_2 , revealing that the dynamic relaxation of supercooled water at AP and above the WL can be described by the excess entropy of its structure.

For both models, the curve of τ_x^{-1} at q_1 is similar as that of τ_s^{-1} , indicating that the two relaxation times are of the same order of magnitude and have the same dependence on excess entropy. This is intriguing, because τ_x is only related to molecular translational motions but τ_s is associated with both translations and reorientations of molecule. Studied with TIP4P/2005 model [93], diffusion coefficients individually associated with translations and reorientations of molecule are decoupled in deeply supercooled regime and violate the Stokes-Einstein relation and the Stokes-Einstein-Debye relation, respectively. Indicated by a recent experiment [94], the violation of the Stokes-Einstein relation is more significant; this violation is attributed to translational jump motions, signified by another simulation study with TIP4P/2005 model [95].

The curve of τ_x^{-1} at q_2 in Fig. 10 shifts upwardly relative to that of τ_x^{-1} at q_1 . Generally, τ_x of the SISF is proportional to $S(q)/q^2$ [35] so τ_x at q_2 is shortened as compared with that at q_1 , though the

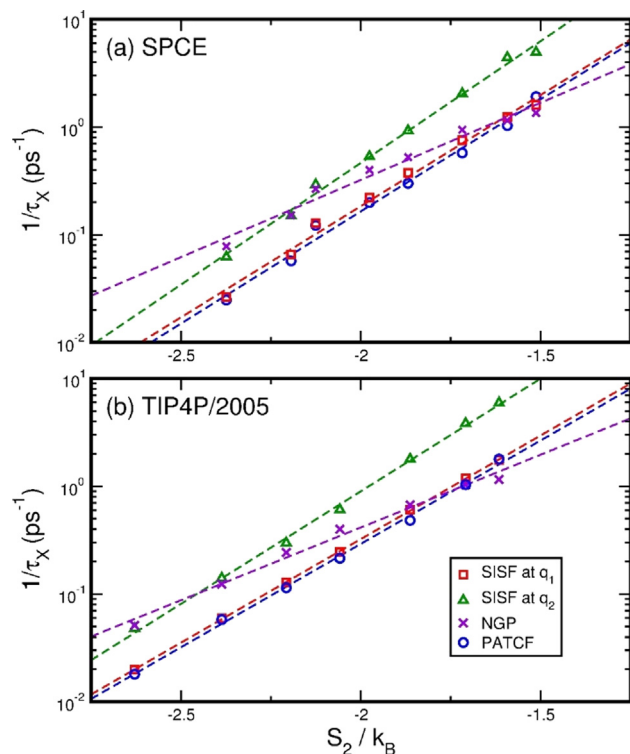


Fig. 10. Inverse relaxation time τ_x^{-1} versus two-body excess entropy S_2 for SPC/E (a) and TIP4P/2005 (b) models at 1 atm. The symbols are simulation data for τ_x^{-1} of the SISF at q_1 (squares), τ_x^{-1} of the SISF at q_2 (triangles), τ_{NG}^{-1} of the NGP maximum (crosses), τ_x^{-1} of the PATCF (circles). The values of S_2 are the data given in Fig. 9 (a). The dashed lines are the fitting results by using Eq. (7).

second peak of $S(q)$ is higher. However, the case of τ_{NG}^{-1} is naïve. For both models, the fitting line of τ_{NG}^{-1} has a slope smaller than those of τ_x^{-1} at q_1 and at q_2 and, therefore, intersects with them at higher and lower S_2 , respectively. Thus, τ_{NG} is of the order of τ_x at q_1 at high temperatures but comparable to τ_x at q_2 at supercooled conditions. This is consistent with that the maximum of the NGP occurs around the end of the β -relaxation, which period substantially increases in time with decreasing temperature [33].

With the partial radial distribution functions shown in Fig. 4 and Fig. S3 [73], the pair entropies S_2^{HH} , S_2^{LL} , and S_2^{HL} were calculated via Eq. (11), and the results of SPC/E and TIP4P/2005 models are shown in Fig. 11 (a) and (b), respectively. Both S_2^{LL} and S_2^{HL} decrease monotonically with temperature, indicating that the structure of LDL becomes more stabilized as decreasing temperature. S_2^{HH} is less sensitive to temperature but displays a shallow minimum roughly at TMD, implying that S_2^{HH} is more related to liquid density. As shown in Fig. S6 [73] for SPC/E liquid at 220 K, the molecular ordering in the second shell of $g_{HH}(r)$ and $g_{LL}(r)$ makes a contribution to S_2^{HH} and S_2^{LL} , respectively, whereas vacancies near the interstitial sites in tetrahedral structure sustained by LDL and its mixing with HDL contribute S_2^{LL} and S_2^{HL} , separately.

Table 3

Parameters of the inverse relaxation time τ_x^{-1} as an exponential function of S_2 in Eq. (7). B_x is in the unit of ps^{-1} and given in its logarithmic value.

Model		τ_x^{-1}		τ_s^{-1}		τ_{NG}^{-1}	
		$\ln B_x$	C_x	$\ln B_s$	C_s	$\ln B_{NG}$	C_{NG}
SPC/E	q_1	7.8167	4.7538	7.7907	4.7963	5.4702	3.3002
	q_2	9.6420	5.2040				
TIP4P/2005	q_1	7.7295	4.4287	7.6104	4.2979	5.3413	3.1104
	q_2	9.5185	4.8127				

Presented in Fig. 11 (c) and (d) are the contributions of HDL, LDL, and their mixing to S_2 . At high temperatures, the HDL contribution dominates S_2 . Due to the decrease of f_H on cooling, the HDL contribution becomes less and less in its absolute value (AV) so that its curves in Fig. 11 (c) and (d) look ascendant for their negative values, where the AV of TIP4P/2005 water is smaller than that of SPC/E. The contributions of LDL and the mixing decrease monotonically with temperature, with their AVs increasing, where their temperature dependences can be fitted by using Eq. (9) as well. Near the WL, the contribution of the mixing becomes significant for almost equal fractions of HDL and LDL.

In summary, the two-body excess entropy of supercooled water above the WL exhibits a logarithmical temperature behavior diverging at a temperature below the WL, and the dynamic relaxation times display a power-law temperature dependence as the prediction of the ideal MC theory for fragile liquids. In reality, the relaxation time of supercooled water confined in silica nanopores changes from the power-law temperature dependence to an Arrhenius behavior as for strong liquids below the WL [96], where molecular hopping by thermal activation becomes the dominated relaxation mechanism [90]. Thus, below the WL, the ideal MC theory fails for describing the relaxation time of supercooled water, which is, therefore, unable to be formulated as an exponential function of two-body excess entropy.

5. Conclusions

In this paper, we have investigated the tetrahedral structure up to the second hydration shell of supercooled water at AP and its effects on dynamic relaxation by comparing simulation results of TIP4P/2005 and SPC/E water models. The tetrahedral structure of supercooled water is characterized with the second-peak maximum and a deep first minimum in the radial distribution function $g(r)$ of O-atoms and the reverse order in magnitude of the first two peaks in structure factor $S(q)$. The first peak q_1 of $S(q)$ is mainly contributed from the second shell of $g(r)$ and the second peak q_2 is associated with O-atom density fluctuations caused by the shell structure of $g(r)$. In 3D, the tetrahedral structure creates interstitial vacancies, which play a role analogous to open local structure responsible for the similar anomaly observed in structure factors of soft-core liquids [80,81]. In our analyses, LDL of supercooled water is specified by molecules, which and their neighbors up to the second hydration shell all have four HB-coordinators, and the other molecules are referred as HDL. At temperatures studied, HDL is dominated in the whole liquid and the fraction of LDL is higher in TIP4P/2005 liquid than in SPC/E.

The studied dynamic properties of water include the SISF, the NGP, and the PATCF. The stretched exponents β_x and β_s characterizing the long-time decay of the SISF and the PATCF, respectively, were obtained from simulations. For both water models, our results indicate the temperature dependence of β_x displays a small peak above the WL. The appearance of this peak is attributed to a partial change from HDL to LDL on cooling, as the LDL fraction reaches roughly one fourth of the total in a result of a slight decrease in structural heterogeneity. β_s of the two models were

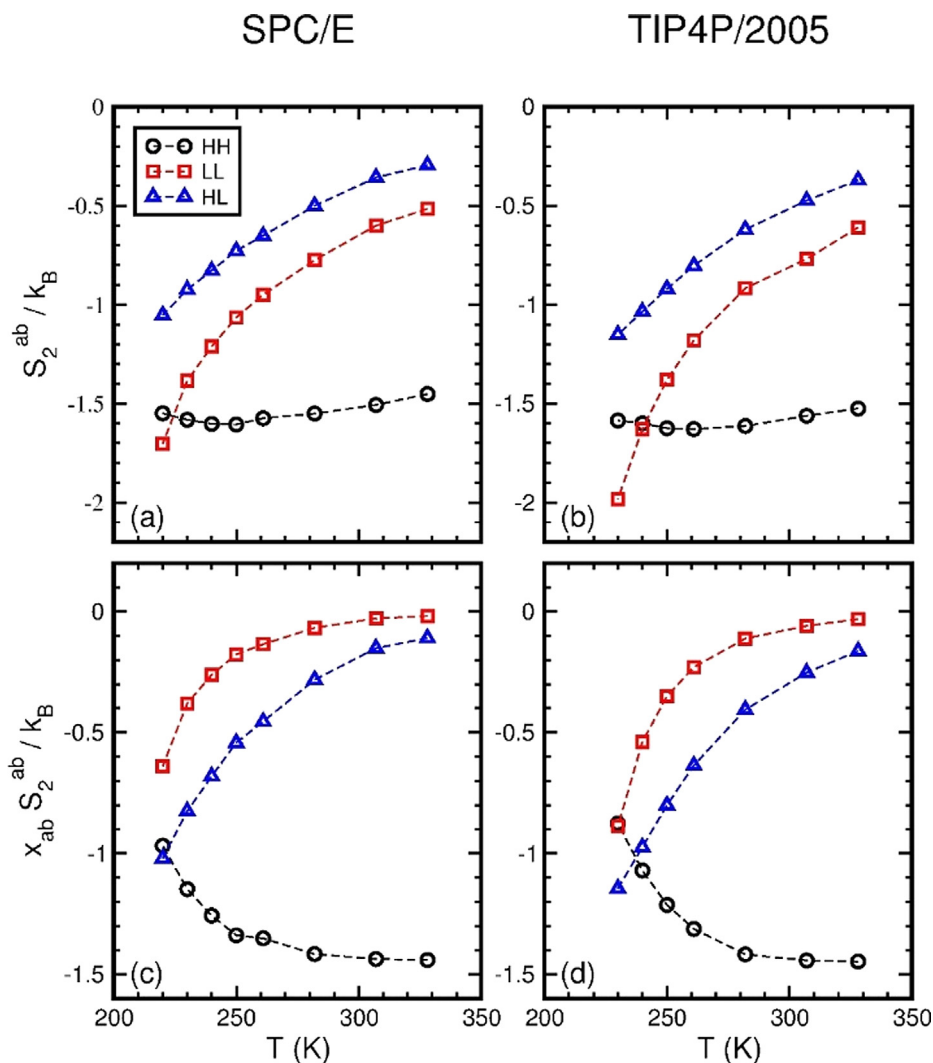


Fig. 11. Partial entropies S_2^{ab} of HDL, LDL, and their mixing (upper panels), and their contributions to two-body excess entropy S_2 (lower panels). The left and right columns are for SPC/E and TIP4P/2005 models at AP, respectively. S_2^{ab} was calculated via Eq. (11) with the partial radial distribution functions $g_{ab}(r)$ shown in Fig. 4 and Fig. S3 [73]. The contributions to S_2 were obtained by multiplying S_2^{ab} with a factor x_{ab} , which is f_H, f_L , and $2\sqrt{f_H f_L}$ for HDL (circles), LDL (squares), and the mixing (triangles), respectively, with f_H and f_L presented in Fig. 3. The dash lines guide the eye for each data set.

found to be insensitive to temperature and both have an average value higher than the experimental data [12,66]. According to our data, β_s has a value more close to β_x at q_2 , rather than at q_1 , in deeply supercooled regime, indicating that the collective polarizability anisotropy of water has a correlation length comparable to the length scale of q_2 , which is slightly smaller than the first-peak distance of $g(r)$.

The relaxation times of the SISFs at q_1 and q_2 , the PATCF, and the maximum of the NGP all display a power-law temperature dependence, with their singular temperatures coincident within a range of 5 K, which is below the WL. Besides γ_{NG} , the critical exponent γ_x characterizing the relaxation time divergence has some relation with local structure and depends on water model, with the SPC/E values higher than the TIP4P/2005 ones in general. As the length scale measuring local structure is shortened, γ_x of the α -relaxation increases with structural heterogeneity and its difference between the two models is enlarged. For the polarizability anisotropy relaxation, γ_s is related to tetrahedral structure of water and its difference between the two models is larger than the differences of γ_x at q_1 and at q_2 , with γ_s of TIP4P/2005 liquid more close to the data of supercooled water [12]. For the NGP, γ_{NG} is almost

the same for the two models, indicating its low association with water structure.

Our results indicate that all inverse relaxation times of supercooled water above the WL can be portrayed as exponential functions of two-body excess entropy S_2 due to translational motions, where S_2 displays a logarithmical divergence at a temperature close to that of relaxation time. At high temperatures, S_2 is resulted from the exclusion volume occupied by a molecule and the tetrahedral order of molecules within the first shell of $g(r)$. In the supercooled regime, extra contributions come from the tetrahedral order extending up to the second hydration shell and vacancies near interstitial sites in the structure sustained by LDL and its mixing with HDL. Near the WL, the mixing of HDL and LDL contributes to S_2 significantly. The formalism based on two-body excess entropy is applicable for describing dynamic relaxation times of water at AP and above the WL, where HDL is dominated and the density variation of the whole liquid is small. But, in the density region, where the tetrahedral structure makes its thermodynamic anomalies significant, the dynamic relaxation of water is described by other approach, like the Adam-Gibbs relation [97], which has been tested for TIP4P/2005 and SPC/E water models [98,99].

CRediT authorship contribution statement

Yu-Wei Kuo: Software, Formal analysis, Data curation. **Ping-Han Tang:** Methodology, Software, Formal analysis, Data curation. **Hao Wang:** Software, Data curation. **Ten-Ming Wu:** Conceptualization, Methodology, Formal analysis, Writing – original draft, Writing – review & editing. **Shinji Saito:** Conceptualization, Writing – original draft, Writing – review & editing.

Declaration of Competing Interest

The authors declare that they have no known competing financial interests or personal relationships that could have appeared to influence the work reported in this paper.

Acknowledgments

TM Wu acknowledges Ministry of Science and Technology, Taiwan R.O.C. for supports under Grant No. MOST 109-2112-M-009-010. S Saito acknowledges the Japan Society for the Promotion of Science KAKENHI (Grant No. JP21H04676).

Appendix A. Supplementary data

Supplementary data to this article can be found online at <https://doi.org/10.1016/j.molliq.2021.117269>.

References

- [1] F. Franks, *Water: A Matrix of Life*, Royal Soc. of Chemistry, Cambridge, 2000.
- [2] P.G. Debenedetti, *J. Phys., Condens. Matter*. 15 (2003) R1669.
- [3] P.G. Debenedetti, H.E. Stanley, *Phys. Today* 56 (2003) 40.
- [4] R.J. Speedy, C.A. Angell, *J. Chem. Phys.* 65 (1976) 851.
- [5] S. Sastry, P.G. Debenedetti, F. Sciortino, H.E. Stanley, *Phys. Rev. E* 53 (1996) 6144.
- [6] R.J. Speedy, *J. Phys. Chem.* 86 (1982) 982.
- [7] P. Chitnelawong, F. Sciortino, P.H. Poole, *J. Chem. Phys.* 150 (2019) 234502.
- [8] C.A. Angell, *Science* 319 (2008) 582.
- [9] P.H. Poole, F. Sciortino, U. Essmann, H.E. Stanley, *Nature* 360 (1992) 324.
- [10] A.K. Soper, M.A. Ricci, *Phys. Rev. Lett.* 84 (2000) 2881.
- [11] A. Nilsson, L.G.M. Pettersson, *Chem. Phys.* 389 (2011) 1.
- [12] A. Taschin, P. Bartolini, R. Eramo, R. Righini, R. Torre, *Nature Commun.* 4 (2013) 2401.
- [13] R. Shi, H. Tanaka, *J. Am. Chem. Soc.* 142 (2020) 2868.
- [14] E.B. Moore, V. Molinero, *J. Chem. Phys.* 130 (2009) 244505.
- [15] K. Wikfeldt, A. Nilsson, L.G.M. Pettersson, *Phys. Chem. Chem. Phys.* 13 (2011) 19918.
- [16] J. Russo, H. Tanaka, *Nature Commun.* 5 (2014) 3556.
- [17] S. Saito, B. Bagchi, I. Ohmine, *J. Chem. Phys.* 149 (2018) 124504.
- [18] P. Gallo, K. Amann-Winkel, C.A. Angell, M.A. Anisimov, F. Caupin, C. Chakravarty, E. Lascaris, T. Loerting, A.Z. Panagiotopoulos, J. Russo, J.A. Sellberg, H.E. Stanley, H. Tanaka, C. Vega, L.M. Xu, L.G.M. Pettersson, *Chem. Rev.* 116 (2016) 7463.
- [19] J.C. Palmer, P.H. Poole, F. Sciortino, P.G. Debenedetti, *Chem. Rev.* 118 (2018) 9129.
- [20] J.W. Biddle, R.S. Singh, E.M. Sparano, F. Ricci, M.A. González, C. Valeriani, J.L.F. Abascal, P.G. Debenedetti, M.A. Anisimov, F. Caupin, *J. Chem. Phys.* 146 (2017) 034502.
- [21] L. Xu, P. Kumar, S.V. Buldyrev, S.H. Chen, P.H. Poole, F. Sciortino, H.E. Stanley, *Proc. Natl. Acad. Sci. U.S.A.* 102 (2005) 16558.
- [22] A. Nilsson, L.G.M. Pettersson, *Nature Commun.* 6 (2015) 8998.
- [23] J.C. Palmer, F. Martelli, Y. Liu, R. Car, A.Z. Panagiotopoulos, P.G. Debenedetti, *Nature* 510 (2014) 385.
- [24] O. Mishima, H.E. Stanley, *Nature* 396 (1998) 329.
- [25] T.A. Kesselring, G. Franzese, S.V. Buldyrev, H.J. Herrmann, H.E. Stanley, *Sci. Rep.* 2 (2012) 474.
- [26] P.G. Debenedetti, F. Sciortino, G.H. Zerze, *Science* 369 (2020) 289.
- [27] K.H. Kim, A. Späh, H. Pathak, F. Perakis, D. Mariedahl, K. Amann-Winkel, J.A. Sellberg, J.H. Lee, S. Kim, J. Park, K.H. Nam, T. Katayama, A. Nilsson, *Science* 358 (2017) 1589.
- [28] J.A. Sellberg, C. Huang, T.A. McQueen, N.D. Loh, H. Laksmono, D. Schlesinger, R. G. Sierra, D. Nordlund, C.Y. Hampton, D. Starodub, D.P. DePonte, M. Beye, C. Chen, A.V. Martin, A. Barty, K.T. Wikfeldt, T.M. Weiss, C. Caronna, J. Feldkamp, L.B. Skinner, M.M. Seibert, M. Messerschmidt, G.J. Williams, S. Boutet, L.G. Pettersson, M.J. Bogan, A. Nilsson, *Nature* 510 (2014) 381.
- [29] H. Pathak, J. Palmer, D. Schlesinger, K.T. Wikfeldt, J.A. Sellberg, L.G. Pettersson, A. Nilsson, *J. Chem. Phys.* 145 (2016) 134507.
- [30] H. Pathak, A. Späh, N. Esmaeildoost, J.A. Sellberg, K.H. Kim, F. Perakis, K. Amann-Winkel, M. Ladd-Parada, J. Koliyadu, T.J. Lane, C. Yang, H.T. Lemke, A.R. Oggenfuss, P.J.M. Johnson, Y. Deng, S. Zerdane, R. Mankowsky, P. Beaud, A. Nilsson, *Proc. Natl. Acad. Sci. USA* 118 (2021) e2018379118.
- [31] K.H. Kim, K. Amann-Winkel, N. Giovambattista, A. Späh, F. Perakis, H. Pathak, M.L. Parada, C. Yang, D. Mariedahl, T. Eklund, T.J. Lane, S. You, S. Jeong, M. Weston, J.H. Lee, I. Eom, M. Kim, J. Park, S.H. Chun, P.H. Poole, A. Nilsson, *Science* 370 (2020) 978.
- [32] P. Gallo, F. Sciortino, P. Tartaglia, S.H. Chen, *Phys. Rev. Lett.* 76 (1996) 2730.
- [33] F. Sciortino, P. Gallo, P. Tartaglia, S.H. Chen, *Phys. Rev. E* 54 (1996) 6331.
- [34] S.H. Chen, P. Gallo, F. Sciortino, P. Tartaglia, *Phys. Rev. E* 56 (1997) 4231.
- [35] F. Starr, F. Sciortino, H.E. Stanley, *Phys. Rev. E* 60 (1999) 6757.
- [36] P. Gallo, M. Rovere, E. Spohr, *Phys. Rev. Lett.* 85 (2000) 4317.
- [37] Y. Rosenfeld, *Phys. Rev. A* 15 (1997) 2545.
- [38] Y. Rosenfeld, *J. Phys.: Condens. Matter* 11 (1999) 5415.
- [39] M. Dzugutov, *Nature* 381 (1996) 137.
- [40] J. Mittal, J.R. Errington, T.M. Truskett, *J. Phys. Chem. B* 110 (2006) 18147.
- [41] Z. Yan, S.V. Buldyrev, H.E. Stanley, *Phys. Rev. E* 78 (2008) 051201.
- [42] J.C. Dyre, *J. Chem. Phys.* 149 (2018) 210901.
- [43] R. Chopra, T.M. Truskett, J.R. Errington, *J. Chem. Phys.* 133 (2010) 104506.
- [44] A. Banejee, S. Sengupta, S. Sastry, S.M. Bhattacharyya, *Phys. Rev. Lett.* 113 (2014) 225701.
- [45] P. Gallo, M. Rovere, *Phys. Rev. E* 91 (2015) 012107.
- [46] M. De Marzio, G. Camisasca, M.M. Conde, M. Rovere, P. Gallo, *J. Chem. Phys.* 146 (2017) 084505.
- [47] A. Rahman, *Phys. Rev.* 136 (1964) A405.
- [48] P. Bartolini, A. Taschin, R. Eramo, R. Torre, *Time-Resolved Spectroscopy in Complex Liquids*, edited by R. Torre, Springer, New York, 2008 (Chapter 2).
- [49] J.L.F. Abascal, C. Vega, *J. Chem. Phys.* 123 (2005) 234505.
- [50] H.J.C. Berendsen, J.R. Grigera, T.P. Straatsma, *J. Phys. Chem.* 91 (1987) 6269.
- [51] N. Giovambattista, T. Loerting, B.R. Lukanov, F.W. Starr, *Sci. Rep.* 2 (2012) 390.
- [52] A. Scala, F.W. Starr, E. La Nave, H.E. Stanley, F. Sciortino, *Phys. Rev. E* 62 (2000) 8016.
- [53] P.H. Tang, T.M. Wu, *J. Mol. Liq.* 301 (2020) 112363.
- [54] A.M. Saitta, F. Datchi, *Phys. Rev. E* 67 (2003) 020201.
- [55] F. Perakis, G. Camisasca, T.J. Lane, A. Späh, K.T. Wikfeldt, J.A. Sellberg, F. Lehmkuhler, H. Pathak, K.H. Kim, K. Amann-Winkel, S. Schreck, S. Song, T. Sato, M. Sikorski, A. Eilert, T. McQueen, H. Ogasawara, D. Nordlund, W. Roseker, J. Koralek, S. Nelson, P. Hart, R. Alonso-Mori, Y. Feng, D. Zhu, A. Robert, G. Grübel, L.G.M. Pettersson, A. Nilsson, *Nat Commun.* 9 (2018) 1917.
- [56] M. Paolantoni, B.M. Ladanyi, *J. Chem. Phys.* 117 (2002) 3856.
- [57] M.D. Elola, B.M. Ladanyi, *J. Phys. Chem. B* 110 (2006) 15525.
- [58] A.A. Milischuk, B.M. Ladanyi, *J. Phys. Chem. B* 117 (2013) 15729.
- [59] J.P. Hanson, I.R. McDonald, *Theory of Simple Liquids*, 2nd ed., Academic Press, London, 1986.
- [60] W. Götz, *Complex Dynamics of Glass-Forming Liquids: A Mode-Coupling Theory*, Oxford University Press, Oxford, 2009.
- [61] W. Kob, H.C. Andersen, *Phys. Rev. E* 51 (1995) 4626.
- [62] S. Saito, I. Ohmine, *J. Chem. Phys.* 106 (1997) 4889.
- [63] S. Saito, I. Ohmine, *J. Chem. Phys.* 108 (1998) 240.
- [64] P.H. Tang, T.M. Wu, *J. Mol. Liq.* 269 (2018) 38.
- [65] S. Saito, I. Ohmine, *J. Chem. Phys.* 102 (1995) 3566.
- [66] R. Torre, P. Bartolini, R. Righini, *Nature* 428 (2004) 296.
- [67] A. Baranyai, D.J. Evans, *Phys. Rev. A* 40 (1989) 3817.
- [68] K.H. Tsai, T.M. Wu, *Comput. Phys. Commun.* 182 (2011) 62.
- [69] S. Plimpton, *J. Comput. Phys.* 117 (1995) 1.
- [70] S.A. Nosé, *J. Chem. Phys.* 81 (1984) 511.
- [71] W.G. Hoover, *Phys. Rev. A* 31 (1985) 1695.
- [72] M.P. Allen, D.J. Tildesley, *Computer Simulation of Liquids*, Clarendon Press, Oxford, 1987.
- [73] See **Supplemental Materials**.
- [74] C. Vega, J.L.F. Abascal, *Phys. Chem. Chem. Phys.* 13 (2011) 19663.
- [75] L.B. Skinner, C.J. Benmore, J.C. Neufeld, J.B. Parise, *J. Chem. Phys.* 141 (2014) 214507.
- [76] H. Pathak, A. Späh, K.H. Kim, I. Tsironi, D. Mariedahl, M. Blanco, S. Huotari, V. Honkimaki, A. Nilsson, *J. Chem. Phys.* 150 (2019) 224506.
- [77] S. Saito, B. Bagchi, *J. Chem. Phys.* 150 (2019) 054502.
- [78] R. Shi, H. Tanaka, *Sci. Adv.* 5 (2019) eaav3194.
- [79] S. Saito, I. Ohmine, B. Bagchi, *J. Chem. Phys.* 138 (2013) 094503.
- [80] G. Franzese, G. Malescio, A. Skibinsky, S. Bulderev, H.E. Stanley, *Phys. Rev. E* 66 (2002) 051206.
- [81] P. Vilaseca, G. Franzese, *J. Chem. Phys.* 133 (2010) 084507.
- [82] J.R. Errington, P.G. Debenedetti, *Nature* 409 (2001) 318.
- [83] The HB of a donor-acceptor pair is defined as that the O-O distance of the molecular pair is less than that corresponding to the first minimum of and the angle between the OH of the donor and the O-O vector of the pair is less than .
- [84] P.J. Steinhardt, D.R. Nelson, M. Ronchetti, *Phys. Rev. B* 28 (1983) 784.
- [85] W. Lechner, C. Dellago, *J. Chem. Phys.* 129 (2008) 114707.
- [86] T.A. Kesselring, E. Lascaris, G. Franzese, S.V. Buldyrev, H.J. Herrmann, H.E. Stanley, *J. Chem. Phys.* 138 (2013) 244506.
- [87] M. Matsumoto, T. Yagasaki, H. Tanaka, *Phys. Rev. Lett.* 115 (2015) 197801.
- [88] M.D. Ediger, *Annu. Rev. Phys. Chem.* 51 (2000) 99.
- [89] The peak high is defined as the difference between at the peak and that at the minimum.
- [90] K. Ito, C.T. Moynihan, C.A. Angell, *Nature* 398 (1999) 492.
- [91] C.A. Angell, J. Shuppert, J.C. Tucker, *J. Phys. Chem.* 77 (1973) 3092.

- [92] T. Lazaridis, M. Karplus, *J. Chem. Phys.* 105 (1996) 4294.
[93] T. Kawasaki, K. Kim, *Sci. Rep.* 9 (2019) 8118.
[94] A. Dehaoui, B. Isenmann, F. Caupin, *Proc. Natl. Acad. Sci.* 112 (2015) 12020.
[95] S. Dueby, V. Dubey, S. Daschakraborty, *J. Phys. Chem. B* 123 (2019) 7178.
[96] L. Liu, S.H. Chen, A. Faraone, C.W. Yen, C.Y. Mou, *Phys. Rev. Lett.* 95 (2005) 117802.
[97] G. Adam, J.H. Gibbs, *J. Chem. Phys.* 43 (1965) 139.
[98] P.H. Handle, F. Sciortino, *Mol. Phys.* 116 (2018) 3366.
[99] A. Scala, F.W. Starr, E. La Nave, F. Sciortino, H.E. Stanley, *Nature* 406 (2000) 166.